HHS Public Access

Author manuscript

Simul Synth Med Imaging. Author manuscript; available in PMC 2021 October 01.

Published in final edited form as:

Simul Synth Med Imaging. 2020 October ; 12417: 184–194. doi:10.1007/978-3-030-59520-3_19.

Auditory Nerve Fiber Health Estimation Using Patient Specific Cochlear Implant Stimulation Models

Ziteng Liu, **Ahmet Cakir**, **Jack H. Noble**

Department of Electrical Engineering and Computer Science, Vanderbilt University, Nashville, TN 37235, USA

Abstract

Cochlear implants (CIs) restore hearing using an array of electrodes implanted in the cochlea to directly stimulate auditory nerve fibers (ANFs). Hearing outcomes with CIs are dependent on the health of the ANFs. In this research, we developed an approach to estimate the health of ANFs using patient-customized, image-based computational models of CI stimulation. Our stimulation models build on a previous model-based solution to estimate the intra-cochlear electric field (EF) created by the CI. Herein, we propose to use the estimated EF to drive ANF models representing 75 nerve bundles along the length of the cochlea. We propose a method to detect the neural health of the ANF models by optimizing neural health parameters to minimize the sum of squared differences between simulated and the physiological measurements available via patients' CIs. The resulting health parameters provide an estimate of the health of ANF bundles. Experiments with 8 subjects show promising model prediction accuracy, with excellent agreement between neural stimulation responses that are clinically measured and those that are predicted by our parameter optimized models. These results suggest our modeling approach may provide an accurate estimation of ANF health for CI users.

Keywords

Cochlear implant; Auditory nerve fibers; Optimization

1 Introduction

Cochlear implants (CIs) are considered the standard-of-care treatment for profound sensory-based hearing loss. In normal hearing, sound waves induce pressure oscillations in the cochlear fluids, which in turn initiate a traveling wave of displacement along the basilar membrane (BM). This membrane divides the cochlea along its length and produces maximal response to sounds at different frequencies [1]. Because motion of BM is then sensed by hair cells which are attached to the BM, these sensory cells are fine-tuned to respond to different frequencies of the received sounds. The hair cells further pass signals to auditory nerve fibers (ANFs) by releasing chemical transmitters. Finally, the electrical stimulation is propagated along the ANFs to the auditory cortex allowing the brain to sense and process the sounds.

ziteng.liu@vanderbilt.edu.

For patients suffering sensorineural hearing loss, which is principally caused by damage or destruction of the hair cells, direct stimulation of the auditory nerve using a CI is possible if ANFs are intact [2]. A CI replaces the hair cells with an externally worn signal processor that decomposes the incoming sound into signals sent to an electrode array that is surgically implanted into the cochlea (see Fig. 1a). Electrode arrays have up to 22 contacts depending on the manufacturer, dividing the available ANFs to, at most, 22 frequency bands or stimulation areas when using monopolar stimulation. Studies have shown that hearing outcomes with CIs are dependent on several factors including how healthy the ANFs are [14]. After surgery, CI recipients undergo many programming sessions with an audiologist who adjusts the settings for every single electrode to improve overall hearing performance. However, lacking objective information about ANF health and more generally about what settings will lead to better performance, a trial and error procedure is implemented. As weeks of experience with given settings are needed to indicate long-term outcome with those settings, this process can be frustratingly long and lead to suboptimal outcomes.

Our group has been developing image-guided CI programming techniques (IGCIP) in order to provide objective information that can assist audiologists with programming [3–5]. Although IGCIP has led to better hearing outcomes in experiments [4, 5], neural stimulation patterns of the electrodes are estimated in a coarse manner using only the distance from each electrode to the neural activation sites in our current implementation. So, it is possible that the method could be improved with a better estimate of the electrodes' neural activation patterns with a physics-based model. To achieve that, we developed patient-specific models of the electrically stimulated cochlea [6, 7] which allow us to estimate intra-cochlear electric fields (EF) created by the CI for individual patients. Building on those studies, in this study we propose to use these EF models as input to ANF activation models to predict neural activation caused by electrical stimulation with the CI. We also propose the first *in vivo* approach to estimate the health of individual ANFs for CI patients using these models.

In summary, herein we propose patient-customized, image-based computational models of ANF stimulation. We also present a validation study in which we verify the model accuracy by comparing its predictions to clinical neural response measurements. Our methods provide patient-specific estimation of the electro-neural interface in unprecedented detail and could enable novel programming strategies that significantly improve hearing outcomes with CIs.

2 Related Works

Several groups have proposed methods for predicting neural activation caused by electrical stimulation [11, 16, 17]. Most of these methods use physiologically-based active membrane nerve models driven by physics-based estimation of the voltage distribution within a given anatomical structure. However, these studies either lack the capacity to be applied in-vivo or only confine themselves to anatomical customization instead of constructing both anatomically and electrically customized models that take advantage of physiological measurements that are clinically available. It is possible that these models need to be fully customized in order to prove useful for clinical use. Thus, in this work we are proposing patient-customized, computational ANF stimulation models, which are not only coupled with our patient-specific electro-anatomical models (EAMs) to ensure electrical and

anatomy customization, but also estimate neural health status along the length of cochlea. Our models permit accurately simulating physiological measurements available via CIs.

Our ANF stimulation models are built on three critical components: the biological auditory nerve model proposed by Rattay *et al.* [11], the CT-based high-resolution EAM of the electrically stimulated cochlea [6, 7], and the auditory nerve fiber segmentation proposed by our group [9]. In the following subsections, we will introduce how these models help to describe auditory nerves from biological, electrical, and spatial features respectively. And in Sect. 3, we will illustrate our approach to combine these models and build our novel, health-dependent ANF stimulation models based on them.

2.1 Biological Nerve Model

The model proposed in by Rattay *et al.* [11] introduce three major features that differs from other nerve models. First, they use compartment model which consists of several subunits with individual geometric and electric parameters as shown in Fig. 1b. Second, Ion channel dynamics are described by a modified Hodgkin-Huxley (HH) model, namely, 'warmed' HH (wHH) model. wHH includes sodium, potassium and leakage currents and has the following form:

$$\frac{dV}{dt} = -\left[-g_{Na}m^3h(V - V_{Na}) - g_K n^4(V - V_K) - g_L(V - V_L) + i_{stimulus}\right]/c \tag{1}$$

$$\frac{dm}{dt} = [-(\alpha_m + \beta_m)m + \alpha_m]k \tag{2}$$

$$\frac{dh}{dt} = [-(\alpha_h + \beta_h)h + \alpha_h]k \tag{3}$$

$$\frac{dn}{dt} = [-(\alpha_n + \beta_n)n + \alpha_n]k \tag{4}$$

$$k = 3^{T - 6.3} \tag{5}$$

$$V = V_i - V_e - V_{rest} \tag{6}$$

where V, V_i, V_e and V_{rest} are the membrane, internal, external and resting voltages, and V_{Na}, V_K, and V_L are the sodium, potassium and leakage battery voltages, respectively. g_{Na}, g_K, g_L are the maximum conductance and m, h, n are probabilities with which the maximum conductance is reduced with respect to measured gating data, for sodium, potassium, and leakage, respectively. $i_{stimulus}$ is the current produced by electrode stimulation, and c is the membrane capacity. Finally, α and β are voltage dependent variables that were fitted from measured data, k is the temperature coefficient, and T is temperature in Celsius. With wHH, the gating processes are accelerated (m, h, n are multiplied by 12), which best fit to observed temporal behavior of human auditory nerves compared to the original HH model, and

leakage conductances are multiplied by the factor 10 to simulate 10-fold channel density. Also, the influence of membrane noise is also taken into account in their approach. These features allow the model to simulate the electrically excited auditory nerves in the human cochlea more accurately than models based on animals.

2.2 Electro-Anatomical Model and Auditory Nerve Fiber Segmentation

In a series of previous studies [6, 7], our group created CT-based high-resolution EAMs to determine the patient-specific EF caused by the current injected via CI electrodes. Briefly, this EAM estimates a volumetric map of the EF through the cochlea created by the CI. The EAM is customized for each patient by customizing a conductivity map so that estimated impedances between all combinations of the CI electrodes best match clinical measurements of these quantities (termed Electrical Field Imaging (EFI)). Then the EF can be found by solving Poisson's equation for electrostatics, which is given by $\nabla \cdot J = -\sigma \nabla^2 \Phi$, where Φ is the EF, J is the electric current density and σ is the conductivity. We are able to define the current source and ground for the CI versus other nodes by manipulating the left-hand side of the equation. As it is discussed in [6], the tissue in this model was assumed to be purely resistive, thus the amount of current enters a node equals to the amount of current that leaves the same node. The finite difference method solution to it can be foud by solving $A\vec{\Phi} = \vec{b}$, where A is a sparse matrix containing coefficients of the linear sum of currents equations, $\vec{\Phi}$ are the set of node voltages that are being determined and are concatenated into a vector, and $b(i)$ equals to +1μA if the ith node is a current source and 0 otherwise. The nodes representing ground are eliminated from the system of linear equations, so the net current is not constrained for those nodes. This system of linear equations is then solved by using the bi-conjugate gradient method [6].

The EAMs are electrically customized by optimizing the tissue resistivity estimates to minimize the average error between simulated EFIs and measured EFIs. The resistivity values for different tissue classes, including electrolytic fluid, soft tissues, neural tissue, and bone, are bound to vary in a range of 50 to 150% of their default values, which are 300, 50, 600, and 5000 Ωcm respectively. Figure 2 shows the EFI simulation of a customized EAM and a generic EAM which uses default electrical properties for 4 electrodes of the same subject, demonstrating much better agreement between simulated and measured EFI after customizing electrical properties.

To localize the ANFs, we use a semi-automatic segmentation technique proposed in [8]. That approach relies on prior knowledge of the morphology of the fibers to estimate their position. It treats the fiber localization problem as a path-finding problem [8]. Several points are automatically defined as landmarks using the segmentation of the cochlea. Paths representing 75 fiber bundles that are evenly spaced along the length of the cochlea are then constructed by graph search techniques that gives the shortest path connecting all the landmarks. Because the paths are computed independently and in close proximity, sometimes they overlap or cross. As a post-processing step, manual edits to some of the paths are required. Example results of this process are in Fig. 1a.

3 Methods

We start the methods section with an overview of the proposed approach, followed by subsections providing more detail regarding novel components of the work. There are approximately 30,000 ANFs in a healthy human cochlea [12]. We represent them using auditory nerve bundles that are segmented along the length of the cochlea as shown in Fig. 1a [11]. To reduce the computational cost of our approach, we represent only 75 distinct bundles, each represents potentially hundreds of fibers. Our proposed nerve bundle action potential model is $P_M HM + P_U H(1 - M)$, where P_M and P_U are the action potential responses of single ANF cell biological nerve models (see Sect. 2.1) for a myelinated fiber and the degenerated, unmyelinated fiber model, respectively. H is the number of living fibers in the bundle that can be recruited for stimulation. M is the fraction, among those ANFs, of healthy versus degenerated ones. Thus, the bundle action potential is the superposition of the two fiber model action potential predictions scaled by the number of such fibers we estimate to be present in the bundle. We have designed an approach, described below, to determine patient customized values for these two parameters for each of the 75 distinct bundles.

The biological ANF model permits simulating action potentials (APs) created by ANFs as a result of the EF the ANF is subjected to. The EF sampled at discrete locations along the fiber bundle – each node of Ranvier (black nodes between myelinated segments in Fig. 1b) – is used to drive the ANF activation model. The EF generated by the CI electrodes can drive the ANF models and can be estimated using our CT-based high-resolution EAM of the electrically stimulated cochlea as described in Sect. 2.2.

Next, we will use our bundle model to simulate neural response measurements that can be clinically acquired. These measurements include recordings acquired using the CI electrodes of the combined AP signal that is created by the set of ANFs activated following a stimulation pulse created by the CI. Such measurements are called electrically evoked compound action potentials (eCAPs). Several eCAP-based functions can be clinically acquired. The most common are the amplitude growth function (AGF), which samples how the magnitude of recorded eCAPs (μV) grow as the current is increased for the stimulation pulse signal; and the spread of excitation (SOE) function, which measures the fraction of eCAP responses for two stimulating electrodes that are generated from the same ANFs [9, 10]. Both AGFs and SOEs can be simulated using our models and clinically measured using the patient's implant. While both AGF and SOE are rich with information about the electro-neural interface and have been acquirable for CI patients for decades, these metrics are not routinely used for clinical programming because they have been difficult to interpret. Thus, the method we propose provides a unique opportunity to (1) estimate neural health by tuning model neural health parameters so that model predicted eCAP functions match clinically measured ones; and (2) provide a physical explanation for the AGF and SOE measurements. Both of these typically unknown quantities could significantly improve an audiologist's ability to program the CI.

We tune neural health parameters for each ANF bundle so that simulated AGF functions for each electrode in the array best match the corresponding clinically measured ones. Finally, we conduct a validation study in which we evaluate our health prediction by simulating SOE

functions using the model with the estimated neural health parameters and compare the results to clinical measured SOE to demonstrate the predictive value of our proposed models. The following subsections detail each step of our approach.

3.1 Dataset

N = 8 patients who had undergone CI surgery were used to create neural health estimation models. All the patients underwent pre- and post-implantation CT imaging needed to localize the intra-cochlear position of the electrodes and to create the tissue classification maps for the EAM models. The three clinical electrophysiological measurements critical for tuning and evaluating our models (EFI, AGF, and SOE) were also collected for all electrodes, for all patients with institutional review board approval.

3.2 Nerve Model

For each nerve fiber model, we follow the approach of Rattay *et al.* as we described in Sect. 2.1. We also used the same electrical and geometrical properties as Rattay did in his work [11]. The modeling is done using the NEURON simulation environment [15]. The overview of the auditory nerve fiber used in this study is shown in Fig. 1b. As shown in the figure, each nerve model consists of three subunits which are the peripheral axon, the soma and the central axon. The peripheral axon is located near hair cells in a human cochlea. They are myelinated when the fiber is healthy and fully functional. It is also common in patients with hearing loss that fibers where the peripheral axon has become unmyelinated exist and could have a weaker response to stimulation [14]. We define them as functional but ‘unhealthy’ ANFs. Then we can parameterize the health of each nerve bundle by varying the number of fibers, H, as well as the ratio of myelinated vs unmyelinated fibers, M, for each ANF bundle.

Our bundle model simulates bundle APs to the estimated EF generated by CI electrodes as previously discussed. Subsequently, eCAP measurements can be simulated in the model. To do this, each node of Ranvier for each bundle is treated as a current source, and the same finite difference method in Sect. 2.2 for estimating EF created by the CI is repurposed for estimating the EF created by the APs generated by all the bundles. This is done by defining bundle nodes as current sources corresponding to cross-membrane current. Thus, the result of each bundle model drives a new EAM to estimate the EF created by the ANFs in the cochlea. The value of the EF is then recorded at the site where the recording electrode is located. This process directly simulates the clinical eCAP measurement process.

In summary, the eCAP simulation can be divided into three steps: (1) for a given stimulating electrode, we calculate the EF using an EAM and record the resulting EF at the nodes of Ranvier for each nerve bundle; (2) we use those voltages as input to the neural activation models for both myelinated and unmyelinated nerves to compute our combined nerve bundle AP; and (3) we estimate the EF created by the bundle APs using another EAM, permitting simulated eCAP measurement from the position of recording electrode. In practice, in the final step an EAM can be created independently for each bundle and the compound response at the recording electrode is then given by

$$\text{simulated eCAP} = \sum_{i=1}^{75} P_{M,i} H_i M_i + P_{U,i} H_i (1 - M_i) \quad (8)$$

where $P_{M,i}$ and $P_{U,i}$ represent the value of the EF sampled at the recording electrode for the simulated eCAP of the myelinated and unmyelinated ANF model in the ith nerve bundle, respectively, and H_i and M_i, are the number of fibers and fraction of those fibers that are healthy for the ith nerve bundle.

3.3 Optimization Process

Spoendlin *et al.* [12] found that for a healthy human cochlea, the average number of fibers can vary between 500 fibers per millimeter (mm) to 1400 fiber per mm depending on the location within the cochlea. Given that a nerve bundle in our model can represent a region as wide as 0.4 mm along the length of cochlea, we have set the boundary values for number of functional nerve fibers to be between 0 (all unresponsive) and 550 (all responsive) and the healthy ratio or the myelination ratio from 0 (all responsive nerve fibers are damaged) to 1 (all responsive nerve fibers are healthy).

Algorithm 1.

Estimate the patient specific neural health parameters

Input: $\mathbf{P_{AGF}}$ = Patient AGF measurement

Variables: $\mathbf{S_{AGF}}$ = Simulated AGF data, **H** = Number of nerve fibers within bundles, **M** = Myelination ratio of fibers within bundles

Output: HC = Fiber count assigned to each control point, **MC** = Myelination ratio assigned to each control point

Start: Assign threshold and maxIteration, randomly assign **HC** and **MC**

While $\Delta|error|$ > threshold and counter < maxIteration

  Interpolate **H** and **M** using **HC** and **MC**

Calculate $\mathbf{S_{AGF}}$ using **H** and **M**

For each electrode i

  $error_{\text{AGF}}$ [i] = mean(abs($\mathbf{P_{AGF}}$ [i] - $\mathbf{S_{AGF}}$ [i]))

$error$ = mean($error_{\text{AGF}}$)

  Optimize **HC** and **MC** using a constrained nonlinear search based on Nelder-Mead simplex

Instead of determining values for H_i and M_i for each of the 75 nerve bundles independendy, a set of control points are used to enforce spatial consistency in parameter values. We define n + 1 control points along the length of cochlea, where n is the total number of active electrodes. The control points are positioned to bracket each electrode. The parameters at those control points were randomly initialized with H_i between 0 to 550 and M_i from 0 to 1. The parameters for each nerve bundle are then linearly interpolated along the length of the cochlea using the control points.

We use the bounded Nelder-Mead simplex optimization algorithm [13] to optimize values at the control points. The cost function is calculated as the mean absolute difference between the simulated and measured AGF values for each electrode. Starting from a random initialization at each control point, our algorithm will iteratively calculate the parameters of

every nerve bundle by interpolating control point values, simulate AGF using those parameters to evaluate the cost function discussed above, and determine new control point parameters using the Nelder-Mead simplex method until a maximum iteration number is reached or the change in error falls below the termination threshold (0.1 μV). Algorithm pseudocode is presented in Algorithm 1.

In our implementation, AGF values that were less than 35 μV were not included in the optimization process because low AGF values tend to be below the noise floor and are usually excluded from clinical analyses. During our experiments, Algorithm 1 is executed from 250 different random initializations for each patient model. The final fiber count and healthy ratio for every nerve bundle are determined as the median values across the 10 optimization runs that resulted in the lowest average error. This procedure diminishes the likelihood of choosing sub-optimal parameters that are local minima.

4 Results

The average absolute differences between the simulated and measured AGF and SOE values for fully customized EAMs are shown on the left side of Table 1. The average absolute difference between the simulated and the measured AGF values could be interpreted as the training error. Mann-Whitney U tests reveal significant improvement in AGF errors after training ($p < 0.01$). The error between the simulated and the measured SOE can be interpreted as the testing error since SOE was not used to optimize neural health parameters. Further, SOE is likely more sensitive to neural health than AGF because it is much more dependent on the spatial distribution of ANFs that contribute to the neural responses. The average SOE error across all patients after optimizing neural health parameters using our proposed method is 39.5 μV.

In Fig. 3, we plot the simulation and clinical result of both AGF and SOE for subject 1. Both of the quantitative and qualitative comparisons show excellent agreement between neural stimulation responses that are clinically measured and those that are predicted by our parameter optimized models. We further compare the difference between neural health estimation using our fully customized models vs. generic models, where default electrical properties are used, for the first 5 subjects in the right side of Table 1. The AGF error (training error) resulting from the generic and electrically customized models is similar while the testing error with fully customized models is much smaller than generic models. A one sided Mann-Whitney U test reveals significantly better ($p < 0.05$) testing error with the fully customized model compared to the generic models. Example plots demonstrating the superiority of SOE simulations using customized for one subject are shown in Fig. 4. These results imply our patient-specific EAMs are critical, not only for EFI simulation, but also for accurate neural health estimation. An example neural health estimation result is shown in Fig. 1a, where the neural health color-codes are a combined function of both health parameters equal to $H(0.5 + M)$. Varying health of several regions of nerves was identified by the proposed method in order for prediction to match measured AGF.

5 Conclusion

In this research, we developed an approach to estimate the health of ANFs using patient-customized, image-based computational models of CI stimulation. The resulting health parameters provide an estimate of the health of ANF bundles. It is impossible to directly measure the number of healthy ANFs *in vivo* to validate our estimates, however experiments with 8 subjects show promising model prediction accuracy, with excellent agreement between neural stimulation responses that are clinically measured and those that are predicted by our parameter optimized models. These results suggest our modelling approach may provide accurate estimation of ANF health for CI users. With the current IGCIP approach, assumptions are made about electrical current spread to estimate which fiber groups are activated based on their distance to the electrode. Our estimation on the health of ANFs may improve our estimation of neural stimulation patterns and lead to highly customized IGCIP strategies for patients. Our future work includes evaluating effectiveness of novel patient-customized programming strategies that use these models. Further, our methods could provide an unprecedented window into the health of the inner ear, opening the door for studying population variability and intra-subject neural health dynamics.

Acknowledgements.

This work was supported in part by grant R01DC014037 from the National Institute for Deafness and Other Communication Disorders. The content is solely the responsibility of the authors and does not necessarily represent the official views of this institute.

References

1. Wilson BS, Dorman MF: Cochlear implants: current designs and future possibilities. J. Rehabil. Res. Dev 45(5), 695–730 (2008**)** [PubMed: 18816422] **)**
2. Clark G: Cochlear implants. In: Speech Processing in the Auditory System, pp. 422–462. Springer, New York (2004). 10.1007/0-387-21575-1_8
3. Noble JH, et al.: Image-guidance enables new methods for customizing cochlear implant stimulation strategies. IEEE Trans. Neural Syst. Rehabil. Eng 21(5), 820–829 (2013) [PubMed: 23529109]
4. Noble JH, et al.: Clinical evaluation of an image-guided cochlear implant programming strategy. Audiol. Neurotol 19(6), 400–411 (2014**))**
5. Noble JH, et al.: Initial results with image-guided cochlear implant programming in children. Otol. Neurotol.: Official Publ. Am. Otol. Soc. Am. Neurotol. Soc. Eur. Acad. Otol. Neurotol 37(2), e63 (2016)
6. Cakir A, Dawant BM, Noble JH: Development of a CT-based patient-specific model of the electrically stimulated cochlea. In: Descoteaux M, Maier-Hein L, Franz A, Jannin P, Collins DL, Duchesne S (eds.) MICCAI 2017. LNCS, vol. 10433, pp. 773–780. Springer, Cham (2017). 10.1007/978-3-319-66182-7_88
7. Cakir A, Dwyer RT, Noble JH: Evaluation of a high-resolution patient-specific model of the electrically stimulated cochlea. J. Med. Imaging 4(2), 025003 (2017)
8. Ahmet C, Labadie RF, Noble JH: Auditory nerve fiber segmentation methods for neural activation modeling. In: Medical Imaging 2019: Image-Guided Procedures, Robotic Interventions, and Modeling, vol. 10951. International Society for Optics and Photonics (2019)
9. Briaire JJ, Frijns JHM: Unraveling the electrically evoked compound action potential. Hearing Res. 205(1–2), 143–156 (2005)
10. Hughes M: Objective Measures in Cochlear Implants. Plural Publishing (2012)

11. Rattay F, Lutter P, Felix H: A model of the electrically excited human cochlear neuron: I. Contribution of neural substructures to the generation and propagation of spikes. Hear. Res 153(1–2), 43–63 (2001) [PubMed: 11223296]
12. Spoendlin H, Schrott A: Analysis of the human auditory nerve. Hear. Res 43(1), 25–38 (1989) [PubMed: 2613564]
13. D'Errico J: fminsearchbnd, fminsearchcon (https://www.mathworks.com/matlabcentral/fileexchange/8277-fminsearchbnd-fminsearchcon), MATLAB Central File Exchange. Accessed 16 Aug 2018
14. Nadol JB Jr., Young Y-S, Glynn RJ: Survival of spiral ganglion cells in profound sensorineural hearing loss: implications for cochlear implantation. Ann. Otol. Rhinol. Laryngol 98(6), 411–416 (1989) [PubMed: 2729822]
15. Carnevale NT, Michael LH: The NEURON Book. Cambridge University Press, Cambridge (2006)
16. Cartee LA: Evaluation of a model of the cochlear neural membrane. II: comparison of model and physiological measures of membrane properties measured in response to intrameatal electrical stimulation. Hear. Res 146(1–2), 153–166 (2000). (14) [PubMed: 10913892]
17. Malherbe TK, Hanekom T, Hanekom JJ: Constructing a three-dimensional electrical model of a living cochlear implant user's cochlea. Int. J. Numer. Method Biomed. Eng 32 (7) (2016). 10.1002/cnm.2751

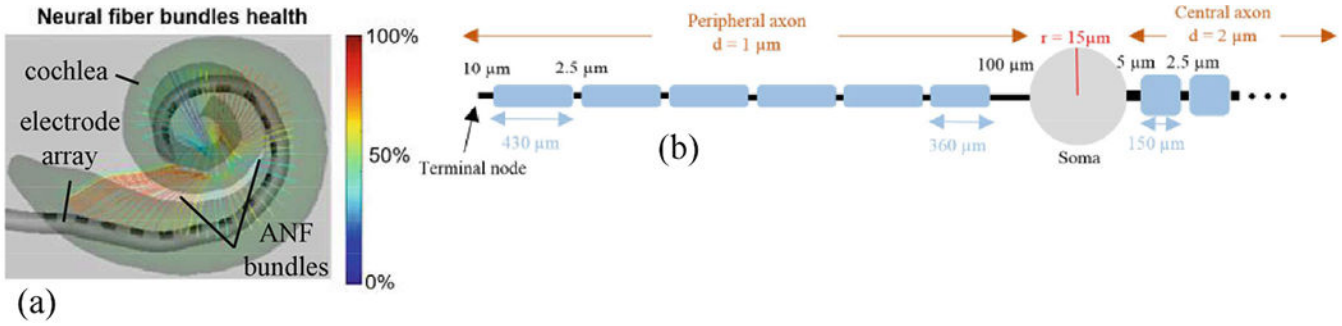

Fig. 1.

Overview of the ANF models. (a) shows the spatial distribution of ANF bundles colored with a nerve health estimate. (b) Shows the ANF stimulation model created for each fiber bundle.

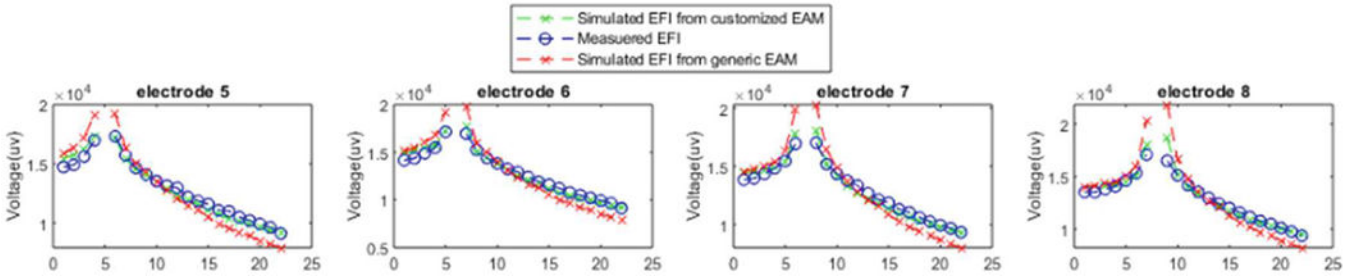

Fig. 2.
EFI simulation of a customized EAM and a generic EAM

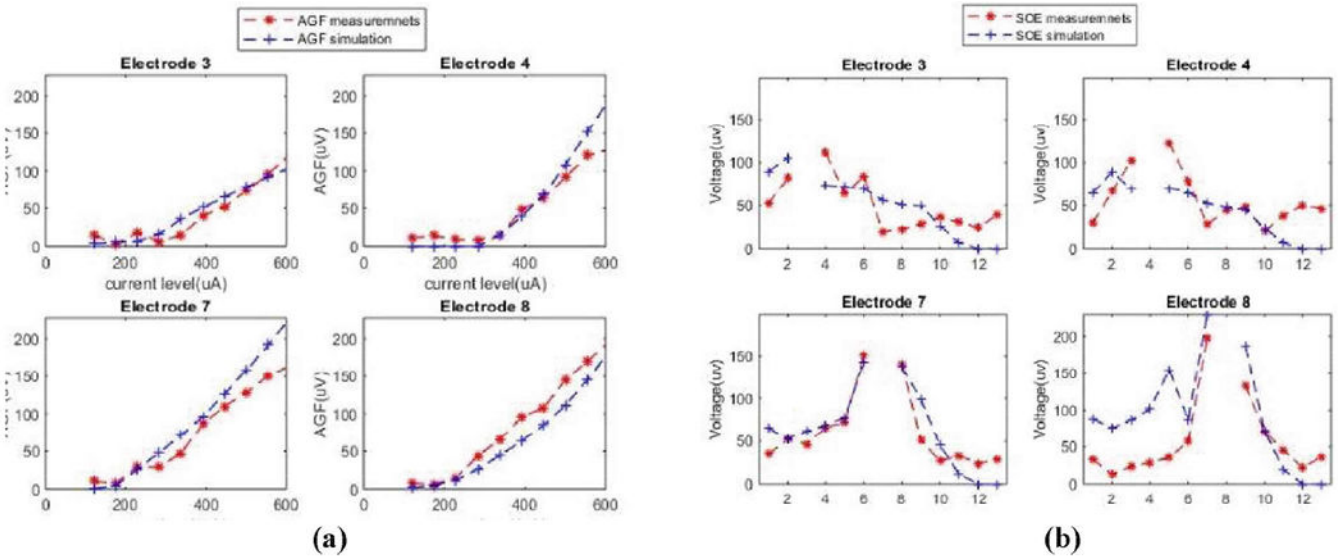

Fig. 3.

(a) Comparison between measured and simulated AGF data. **(b)** Compatison between measured and simulated SOE data

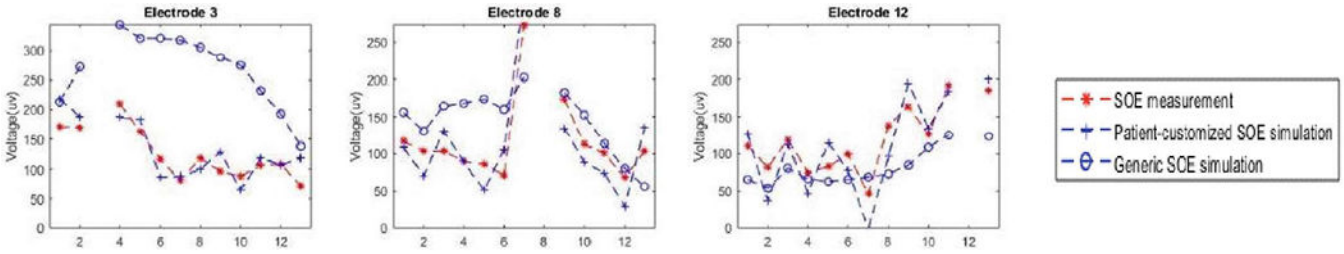

Fig. 4.

SOE testing error for patient-customized versus generic models for Subject 4.

Table 1.

Average mean absolute difference between simulated and measured AGF and SOE.

Subject #	Fully customized models			Generic models	
	AGF error – before optimiz. health (μV)	AGF error – after optimiz. health (μV)	SOE error-testing error (μV)	AGF error – after optimiz. health (μV)	SOE error-testing error (μV)
1	58	16	31	22	53
2	187	19	32	48	49
3	299	39	37	28	76
4	66	37	44	39	102
5	131	11	29	19	56
6	97	8	21	15	36
7	62	17	48	–	–
8	141	26	59	–	–
Average	134	21.6	39.5	28.5	62.0